Research Article

Mary Harli Mol Edwin, Ajin Sundar Sundara Raj, Aravind Mani*, Mika Sillanpää, and Saleh Al-Farraj

Green synthesis of *Vitis vinifera* extract-appended magnesium oxide NPs for biomedical applications

https://doi.org/10.1515/ntrev-2024-0048
received January 25, 2024; accepted June 7, 2024

Abstract: Biologically active magnesium oxide (MgO) nanoparticles were synthesised using green reduction with an extract derived from the *Vitis vinifera* plant. The investigation focused on examining the structure and carbon abundance resulting from the thermal degradation of adsorbed biomolecules. It was accomplished using powder X-ray diffraction, Raman spectroscopy, and FT-IR analysis techniques. X-ray photoelectron spectroscopy studies conducted on MgO nanoparticles indicate the absence of any supplementary peaks, thereby indicating the purity of the material. The morphological characteristics, which have been examined using field emission scanning electron microscopy and TEM methodologies, demonstrate the presence of particles with a spherical shape, exhibiting minimal agglomeration and a uniform distribution across the surfaces of MgO. The porous structure, porosity, and pore volume of the MgO particles were evaluated using Brunauer-Emmett-Teller surface analysis. The experimental findings reveal that the surface area of the MgO nanoparticles is 23.8742 m^2/g, while the total pore volume is 0.12528 cm^3/g. Additionally, the average pore diameter is determined to be 1.7 nm. These observations collectively suggest the presence of microporous structures within the MgO nanoparticles. This article discusses the biological studies to assess the antibacterial, antifungal, anti-inflammatory, and anti-diabetic activities of the synthesised MgO nanoparticles.

Keywords: nanotechnology, nanobiotechnology, antibacterial, antifungal, anti-inflammatory, and anti-diabetic activities.

1 Introduction

Nanomaterials are characterised by their nanoscale dimensions, which enable them to exhibit superior mechanical and electronic properties compared to bulk particles of macroscopic size [1,2]. The subject matter has garnered significant interest recently due to its multifaceted applications across diverse domains, including but not limited to catalysis, gas sensing, energy storage, and energy conversion [3–6]. The preparation of nanomaterials typically involves using two primary methodologies: top-down and bottom-up synthetic routes [7–9]. Recently, a diverse range of nanomaterials has been synthesised chemically to cater to specific applications. Chemical-reducing agents, notably, have garnered increased attention in nanomaterial synthesis [10,11]. Various capping agents and surfactants have been employed in this context [12].

In recent years, using sodium borohydride as a reducing agent has grown more common in the chemical reduction process for synthesising nanomaterials [13]. Following the advent of bio-extract or biomolecule-derived reducing agents, the conventional chemical reagent-based approach was superseded due to its inherent drawbacks. These drawbacks encompassed the generation of pollution through chemical consumption during nanomaterial synthesis, the utilisation of costly reagents, and the lack of sustainability in the overall process. The

* **Corresponding author: Aravind Mani,** Department of Physics, National Engineering College, K.R. Nagar, Kovilpatti, Tamil Nadu, 628503, India, e-mail: aravind-sh@nec.edu.in
Mary Harli Mol Edwin: Research Scholar, Department of Physics, St. Jude's College, Thoothor, Tamil Nadu, 629176, India; Affiliated to Manonmanium Sundaranar University, Tirunelveli, Tamil Nadu, 627012, India
Ajin Sundar Sundara Raj: Department of Physics, St. Jude's College, Thoothor, Tamil Nadu, 629176, India; Affiliated to Manonmanium Sundaranar University, Tirunelveli, Tamil Nadu, 627012, India
Mika Sillanpää: Functional Materials Group, Gulf University for Science and Technology, Mubarak Al-Abdullah, 32093, Kuwait, Kuwait; Adnan Kassar School of Business, Lebanese American University, Beirut, Lebanon; Centre of Research Impact and Outcome, Chitkara University Institute of Engineering and Technology, Chitkara University, Rajpura, 140401, Punjab, India; Division of Research & Development, Lovely Professional University, Phagwara, 144411, Punjab, India
Saleh Al-Farraj: Department of Zoology, College of Science, King Saud University, Riyadh, Saudi Arabia

bio-extracts, which consist of various biomolecules such as polyphenols, alkaloids, and terpenoids, exhibit functional groups that readily coordinate the binding of metal ions. Additionally, these bio-extracts can decrease the particle size by regulating nucleation growth [14,15]. According to numerous reports, many recent publications focus on utilising plant extract-derived reducing agents to synthesise nanoparticles [14–18].

Nanomaterials, in their metallic and oxide states, are extensively employed across various energy, medical, and industrial domains [19,20]. Metallic nanoparticles, with their diverse range of morphological configurations and alloy compositions, have been extensively employed in many industrial applications due to their exceptional mechanical robustness and notable resistance to wear, among other advantageous properties [21]. Additionally, metallic nanoparticles and isotopes have been used in cancer cell treatment [22,23]. In this investigation, metallic nanoparticles composed of Ag, Au, and Pt were primarily examined for their potential applications in biological studies and as inhibitors of carcinogens [24,25]. In a similar vein, the utilisation of metal oxide nanoparticles has garnered significant interest in the fields of energy storage, energy conversion, and biological applications. The effective coupling of nanomaterials has led to significant advancements in various fields, including solar photovoltaics, gas sensors, and LED applications [26–28]. Zinc oxide and titanium dioxide nanomaterials have been extensively studied to predict their biological properties, specifically regarding the bio-reducing agents employed in their synthesis [29,30].

Magnesium oxide (MgO), an amalgamation of magnesium and oxygen, has attracted substantial scrutiny due to its intricate participation in biological investigation. The aforementioned inorganic compound, frequently encountered as a solid mineral with a white appearance, exhibits unique characteristics that render it a subject of considerable fascination across multiple scientific fields, encompassing but not limited to medicine, biochemistry, physiology, and nutrition [31]. The core of its significance resides in magnesium, a vital mineral intricately intertwined with numerous physiological processes within living organisms. Magnesium is widely acknowledged as an essential cofactor in various enzymatic reactions, a key regulator of ion channels, and a crucial stabiliser of DNA and RNA structures. The chemical reaction between magnesium and oxygen, resulting in the formation of MgO, yields a compound that exhibits promising implications for various cellular activities, tissue health, and the overall well-being of organisms [32].

The unique microstructural characteristics of MgO, including its notable porosity, expansive surface area, and presence of acid–base sites, contribute to its surface's remarkable responsiveness in various applications [33]. The diverse morphological configurations exhibited by MgO, including rod-like structures, spherical shapes, platelets, floral arrangements, star-like formations, cubic shapes, and needle-like structures, render them highly suitable for the fabrication of nanomaterials possessing unique and unprecedented properties [34,35]. The proliferation of scientific literature documenting advancements in the field of MgO nanoparticles has exhibited a notable upward trend over time. Multiple studies have demonstrated the utilisation of MgO in photocatalysis, its efficacy as an antimicrobial agent, and its application in energy cells and sensors. Exploring novel biomedical engineering applications involving MgO nanoparticles is an increasing interest and research area. MgO has been found to possess various applications in biomedical research. These applications include tissue regeneration, implant coatings, bioimaging, wound healing, and the development of cancer therapies [36,37].

The report discusses the use of innovative plant extract-reducing agents for synthesising MgO nanoparticles and explores their biological activities. The study highlights the simplicity and potential of the sustainable synthesis method using *Trigonella foenum-graecum* for various biomedical applications. The antibacterial effectiveness of the MgO nanoparticles against Gram-positive and Gram-negative bacteria is observed. Another study focuses on the green synthesis technique using an extract from the leaves of *Pisonia alba* to fabricate magnetic oxide nanoparticles with antioxidant and antifungal properties [38]. The combustion method is utilised in another investigation to synthesise MgO nanoparticles using glutamine and L-arginine as fuels. The biological efficacy of these nanoparticles against bacterial strains and fungi is evaluated [39]. The production of MgO nanoparticles using *Carica papaya* leaf extract and their antimicrobial efficacy against *Bacillus subtilis* is described in a comprehensive account [40]. The green synthesis methodology using *Moringa oleifera* leaves and magnesium chloride solution is examined, and the antibacterial effectiveness of the MgO nanoparticles against *Staphylococcus aureus* and *Escherichia coli* is determined [41]. The reduction of magnesium ions facilitated by the phytochemicals in the leaf extract of *Ajwain (Trachyspermumammi)* is observed, resulting in the formation of oxide nanoparticles with significant biological activity [42]. The antimicrobial characteristics of MgO nanoparticles extracted from *Datura stramonium* leaves against *E. coli* and *S. aureus* are investigated [43]. The synthesis of MgO nanoparticles using extracts from the Texas sage plant (*Leucophyllum frutescens*) as a capping agent and their antibacterial efficacy against *S. aureus* and *E. coli* are evaluated [44]. The report concludes by discussing the green synthesis approach for producing *Moringa* gum-capped MgO nanoparticles and assessing their antioxidant activity, hemolysis potential, cytotoxicity, phytotoxicity, toxicity in zebrafish embryos, and *in vivo* toxicity [45].

The synthesis of MgO nanoparticles utilising *Vitis vinifera* extract as both a reducing and stabilising agent is a sustainable and environmentally beneficial process, providing a green alternative to traditional techniques [46]. The produced nanoparticles demonstrate a range of beneficial qualities, such as antibacterial [47], antifungal [46], anti-inflammatory, and anti-diabetic activities [48]. These features make them promising for prospective applications in treating infectious, inflammatory, and metabolic illnesses. Using *Vitis vinifera* extract to create nanoparticles improves their bioavailability and therapeutic efficacy, capitalising on the health advantages of the botanical extract.

To use nanoparticles for therapeutic purposes, it is necessary to carefully assess their compatibility with living organisms, their safety, and the potential long-term impacts they may have on biological systems. It is essential to examine cytotoxicity, immunogenicity, and stability to determine their suitability for commercialisation. Maximising therapeutic potential relies heavily on targeting specificity [49]. Standardisation and repeatability are crucial to providing uniform nanoparticle characteristics across several batches [50]. Nevertheless, moving from small-scale synthesis in the laboratory to large-scale production presents difficulties regarding scalability, cost efficiency, and adherence to regulations. Efficiently improving the methods of creating nanoparticles, expanding the capacity of production facilities, and adhering to regulatory standards are essential stages in advancing and commercialising nanoparticle-based medical treatments.

The *Vitis vinifera* extract-appended MgO nanoparticles have been found to exhibit antibacterial, antifungal, anti-inflammatory, and anti-diabetic properties. This discovery suggests a wide range of potential therapeutic applications, such as creating new antimicrobial agents, anti-inflammatory medications, and treatments for diabetes. Their ability to perform several functions may result in synergistic effects, leading to improved therapeutic outcomes compared to drugs targeting a single entity [51].

This study contributes to the growing field of nanomedicine by demonstrating the potential of green-synthesized nanoparticles for biomedical applications, such as targeted drug delivery, imaging, and theranostic applications. Using natural product-derived nanoparticles further expands the scope of nanomedicine, emphasising the importance of sustainable and biocompatible nanomaterials in healthcare. The *Vitis vinifera* extract-appended green synthesis of MgO nanoparticles represents an innovative approach with significant contributions to nanotechnology, natural product-based therapeutics, and nanomedicine.

2 Experimental

2.1 Materials and methods

Magnesium nitrate, distilled water, and fresh *Vitis vinifera* leaves are used to synthesize green nanoparticles.

2.1.1 Bioextract preparation from *Vitis vinifera*

Freshly washed leaves of *Vitis vinifera* were exposed to direct sunlight. Subsequently, 10 g of leaves were dissolved in 100 mL of distilled water using a magnetic stirrer-heater and heated at 50–60°C for 60 min. The resulting yellow solution was filtered to obtain the extract using filter sheets.

2.1.2 Synthesis of MgO nanoparticles

About 10 mL of the *Vitis vinifera* extract aqueous leaf extract was added in drops to 50 mL of 0.1 M solution of $Mg(NO_3)_2{\cdot}6H_2O$ in a 250 mL capacity beaker under a constant stirring condition with a magnetic stirrer. The total time consumed for the addition was 12 h. The obtained solid–liquid dispersion was centrifuged at 7,000 rpm for 10 min. After this, the supernatant was discarded, and the residue was washed with deionised water to remove excess $Mg(NO_3){\cdot}6H_2O$ and residual organic molecules. Furthermore, it was dried in an oven at 70°C for 2 h and then calcined in a furnace at 500°C for 3 h to obtain MgO nanoparticles. The obtained particles are collected and labelled as MO1 (Figure 1). In the MO2 samples, the same methodology was followed with 15 mL of *Viti's vinifera* extract.

2.2 Material characterisation

2.2.1 Antibacterial activity

It was tested using the agar diffusion method to see how well MgO nanoparticles killed Gram-negative *Klebsiella*, *Pseudomonas aeruginosa*, Gram-positive *B. subtilis*, and *Staphylococcus albus*. Agar plates were prepared, and the bacterial strains *E. coli* and *S. aureus* were streaked onto the plates using a streaking technique. The plates were rotated at angles of 60° to achieve a uniform dispersion of the inoculum. The prepared and annealed MgO nanoparticles were put into the healthy plates with micropipettes. Each disc held 75 µL/mL. It was done after inoculating the healthy plates with bacteria. The test samples were meticulously administered to guarantee their containment within the wells. The plates were placed in an incubator for

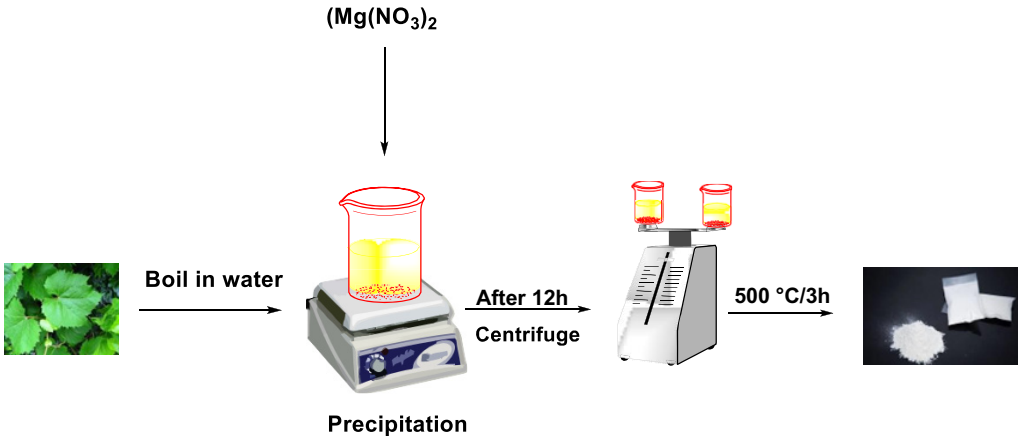

Figure 1: Synthesis of MgO nanoparticles.

24 h at 37°C to facilitate bacteria proliferation and interaction with the test materials. Following incubation, the inhibition areas surrounding the test sample discs were inspected and quantified. The fact that there is a zone of inhibition (ZOI) around the disc shows that the antibacterial properties of the MgO nanoparticles are stopping the growth of bacteria. Positive controls of Amikacin were used to see how well the test samples worked against Gram-negative *Klebsiella* and *Pseudomonas aeruginosa*, as well as Gram-positive *B. subtilis* and *Staphylococcus albus*. These controls aid in establishing a standard for comparing antibacterial activity.

2.2.2 Antifungal activity

The antifungal activity of the synthesised MgO nanoparticles against the fungus *Candida tropicalis* and *Aspergillus niger* was assessed using the agar well diffusion technique. The stock solution was prepared by combining 1 mg of MgO nanoparticles with 1 mL of sterile distilled water. The antibacterial activity assay utilised Muller–Hinton agar plates with a pH of 7.4. About 6 mm-diameter wells were created on the agar plates, into which 100 µL of the synthesised MgO nanoparticles were introduced. The standard control consisted of Nystatin at a 50 µg/mL concentration. After applying the test samples and control to agar plates, incubation was carried out for 18 h at a temperature of 37°C. During the incubation period, the antifungal activity of MgO nanoparticles and the control (Nystatin) both prevented fungal growth in the area around the wells. Afterwards, the diameter of the ensuing transparent area, also referred to as the ZOI was measured once the incubation period had finished. The clear zone corresponds to the region where bacterial growth is suppressed due to the antifungal properties of the test samples or the control. Evaluating the width of the clear zone provides valuable information on the effectiveness of the synthesised MgO nanoparticles in inhibiting fungal growth. A greater clear zone width implies a more potent antifungal action, whereas a more minor or nonexistent clear zone indicates limited or no antifungal activity. By measuring the width of the inhibition zones, this method lets us test and compare how well MgO nanoparticles kill fungus compared to the control substance Nystatin.

2.2.3 Anti-inflammatory activity

The experimental setup involved combining 0.5 mL of the reaction mixture, which comprised 0.4 mL of bovine serum albumin (3% aqueous solution), with different concentrations of the MO2 sample. The sample underwent incubation at a temperature of 37°C for 20 min. Subsequently, a volume of 2.5 mL of phosphate-buffered saline solution with a pH value of 6.3 was introduced into each tube. The tubes were subjected to a thermal treatment at 80°C for 10 min. The absorbance measurement was conducted using a spectrophotometer set at 660 nm. The calculation of the percentage inhibition of protein denaturation was performed in the following equation:

$$\text{Percentage of inhibition} = [(\text{Abs}_{\text{Control}} - \text{Abs}_{\text{Sample}}) / \text{Abs}_{\text{control}}] \times 100. \quad (1)$$

2.3 α-Glucosidase inhibition assay

The impact of the MO2 on α-glucosidase activity was assessed using the methodology outlined by Shai *et al.*, [57] with minor adjustments. A pre-incubation period of 30 min was conducted, during which 400 µL of α-glucosidase with a concentration of 0.067 U/mL was exposed to varying concentrations

of the sample. Subsequently, a volume of 200 µL containing a concentration of 3.0 mM p-nitrophenyl-β-D-glucopyranoside (pNPG), serving as the substrate, was introduced into the experimental setup. The PNP substrate was dissolved in a sodium phosphate buffer at a concentration of 0.1 M and a pH value of 6.9. This addition marked the initiation of the biochemical reaction. The reaction mixture underwent incubation at a temperature of 37°C for 30 min, after which it was terminated by adding 2 mL of sodium carbonate (Na_2CO_3) solution at a concentration of 0.1 M. The α-glucosidase activity was determined by quantifying the para-nitrophenol (pNP) released from pNPG, which exhibited a yellow colour. The measurement was performed at a wavelength of 400 nm. The outcomes were quantified in terms of inhibition percentage. The identical experimental protocol was employed for acarbose (1 mg/mL stock), which served as the reference standard:

$$\text{Inhibitory activity}(\%) = (B - T/B - C) \times 100, \quad (2)$$

where B is the absorbance of the blank, t is the absorbance in the presence of a test substance, and C is the absorbance of the control.

3 Results and discussion

3.1 Structural analyses

3.1.1 Powder X-ray diffraction (PXRD) patterns

The PXRD analysis is performed to enhance comprehension of the structural characteristics of synthesised MO1 and MO2 nanoparticles at different concentrations of the reducing agent, *Viti vinifera* extract. The results obtained are depicted in Figure 2a, which displays the PXRD patterns corresponding to the 2θ values of 37.3°, 43.3°, 62.7°, 75.1°, and 79.0°. The observed peaks correspond to the *hkl* planes with miller indices of (111), (200), (220), (311), and (222), respectively. The observed peaks provide evidence of the presence of MgO in MO1 and MO2 samples that exhibit a face-centred cubic (FCC) structure belonging to the Fm-3m space group. Moreover, the PXRD patterns and their corresponding *hkl* planes are significantly similar to MgO, as reported in the JCPDS card No. 01-075-0447 [52]. No significant alterations in the PXRD pattern were observed when the concentration of the *Vitis vinifera* extract was varied.

Furthermore, the absence of any supplementary peaks observed in the PXRD pattern of MO1 and MO2 indicates the exceptional purity of the MgO nanoparticles. A distinct and pronounced peak observed in the PXRD patterns suggests that the synthesised MgO nanoparticles possess a significant crystallinity level. Metal oxide surfaces exhibit a strong affinity for organic molecules possessing electron acceptor units, such as carboxylic acid, hydroxyl, and pyridyl groups. The bio-extract utilised in the investigation showed an abundance of organic acids, phenolic acids, flavonols, tannins, procyanidins, anthocyanins, and other compounds [53]. Carbon chemisorption on MgO surfaces is readily observed throughout the heat treatment procedure. The surface of the material's activity may undergo significant alteration. The inability to observe this phenomenon in PXRD analysis can be attributed to carbon's amorphous state.

In addition, the FWHM and *d* space values for the as-synthesized nanoparticles are 0.2755 and 2.08445 for MO1,

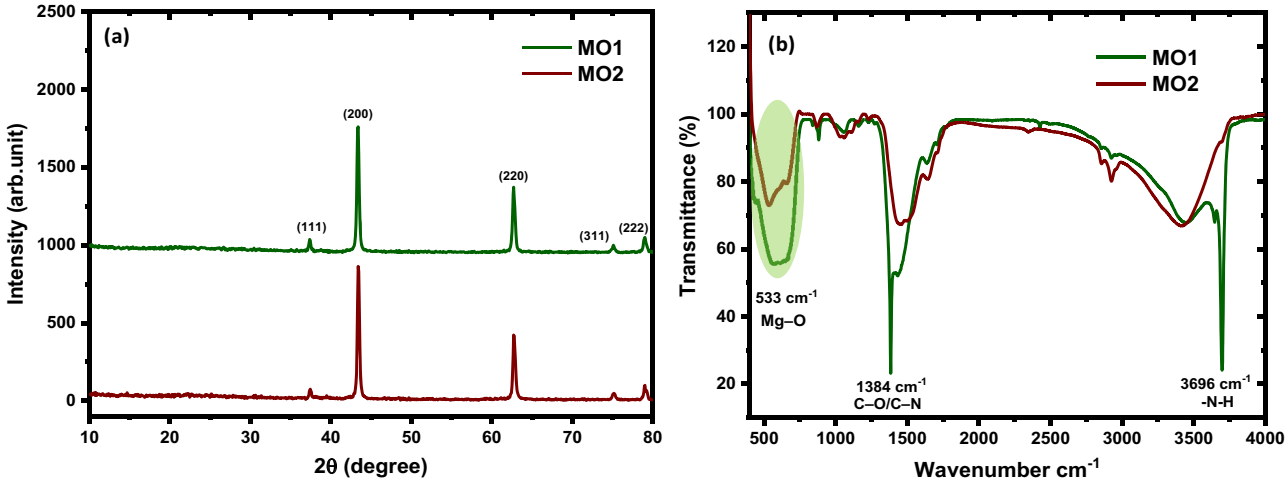

Figure 2: (a) PXRD patterns of MO1 and MO2 nanomaterials, and (b) FT-IR spectra of MO1 and MO2 nanomaterials in KBr standard.

and 0.3444 and 2.08682 for MO2. These two values were changed slightly based on the concentration of the extract used. The high concentration of the extract leads to higher carbon deposited on the MgO surface. This indicated that the *d*-space value was observed to be slightly high, and the FWHM value increased. This could be doping of amorphous carbon from the extract after the thermal treatment at 500°C.

3.1.2 FT-IR investigations

To examine the composition of MgO and the presence of carbon contamination in MO1 and MO2 materials, Fourier transform infrared spectra were obtained using potassium bromide (KBr) as the medium. The results are presented in Figure 2b, wherein a notable peak at 533 cm^{-1} is observed, corresponding to the stretching frequency of Mg–O [54]. In the context of MO1, a distinct peak is observed for MO2 at a wavenumber of 533 cm^{-1}, whereas MO1 exhibits peak broadening. Furthermore, the additional peaks observed at 1,384 and 3,696 cm^{-1} corresponded to the presence of C–N/C–O and −N–H functional groups in the MO1 sample. The data provide clear evidence that the carbon in the MO1 sample can be attributed to the chemisorbed bio-molecules originating from the extract.

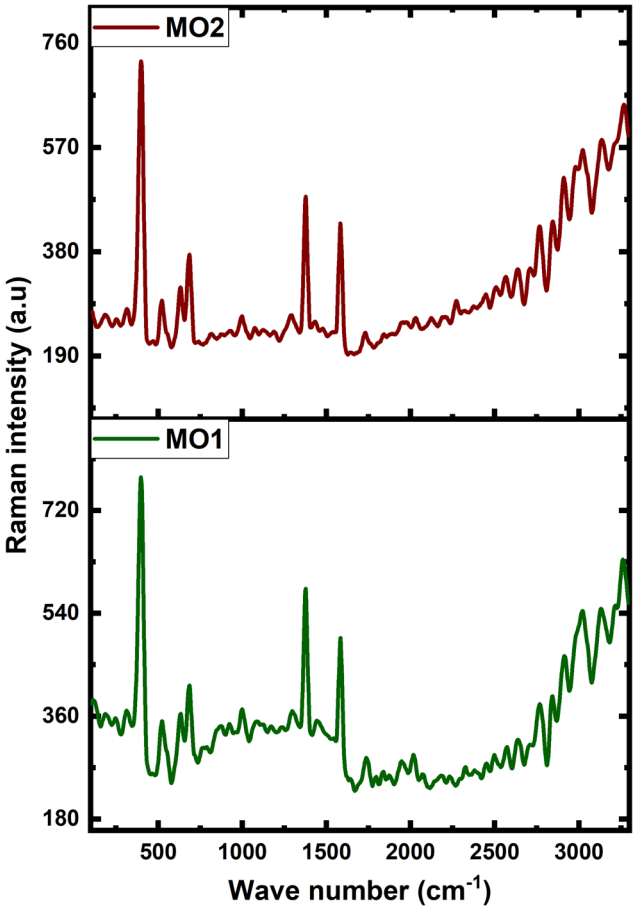

Figure 3: Raman spectra obtained for MO1 and MO2 nanomaterials.

3.1.3 Raman spectral analysis

The Raman spectra were obtained to provide additional evidence for the existence of functional groups and to conduct a structural study of MO1 and MO2. The results are depicted in Figure 3. The observed spectrum displays a distinct peak at 400 cm^{-1}, which can be attributed to the symmetric stretching vibration of oxygen ions (O^{2-}) in the A1g mode of MgO. The Eg mode, which represents the symmetric stretching of oxygen ions along the face-diagonal direction within the cubic lattice, displays a peak at a wavenumber of 632 cm^{-1}. The T1u mode is associated with the stretching vibration of magnesium ions (Mg^{2+}) within the cubic lattice of MgO, resulting in a prominent peak at 522 cm^{-1}. The Eg mode correlates with the symmetric stretching of oxygen ions along a distinct set of axes, separate from the Eg mode. The differentiation between the two can be identified through a distinct peak occurring at approximately 688 cm^{-1}. The Raman spectra of MO1 and MO2 reveal that the G-band displays a spectral range of 1,582 cm^{-1}. This range encompasses the in-plane oscillations of carbon atoms within a hexagonal lattice, as observed in graphite and different crystalline forms of sp^2 hybridised carbon. In the interim, it is noteworthy that the D-band manifests itself at a reduced wavenumber, precisely within the confines of 1,378 cm^{-1}. The quantification of disorder in carbon-based materials is often accomplished by utilising the intensity of the D-band as a reliable indicator. The carbonaceous substance obtained from the extract was found to have accumulated in both the MO1 and MO2 samples, as indicated by the observations made.

3.1.4 X-ray photoelectron spectroscopy (XPS) studies

The XPS spectra were acquired to enhance our understanding of the composition and arrangement of synthesised MgO nanoparticles. The results are depicted in Figure 4, notwithstanding the discernible peaks observed at an energy level of 1305.2 eV to the Mg 1s energy states. The observed peak suggests the MO2 sample contains the Mg^{+} ion in a +1 oxidation state. No additional peaks were observed at 1,300 eV, indicating the absence of further phases of magnesium, such as magnesium hydroxide and complex magnesium structures. The deconvolution spectra of the O 1s exhibit a discernible peak at 530.6 eV, which can be attributed to the presence of oxygen vacancies and chemisorbed oxygen species on the

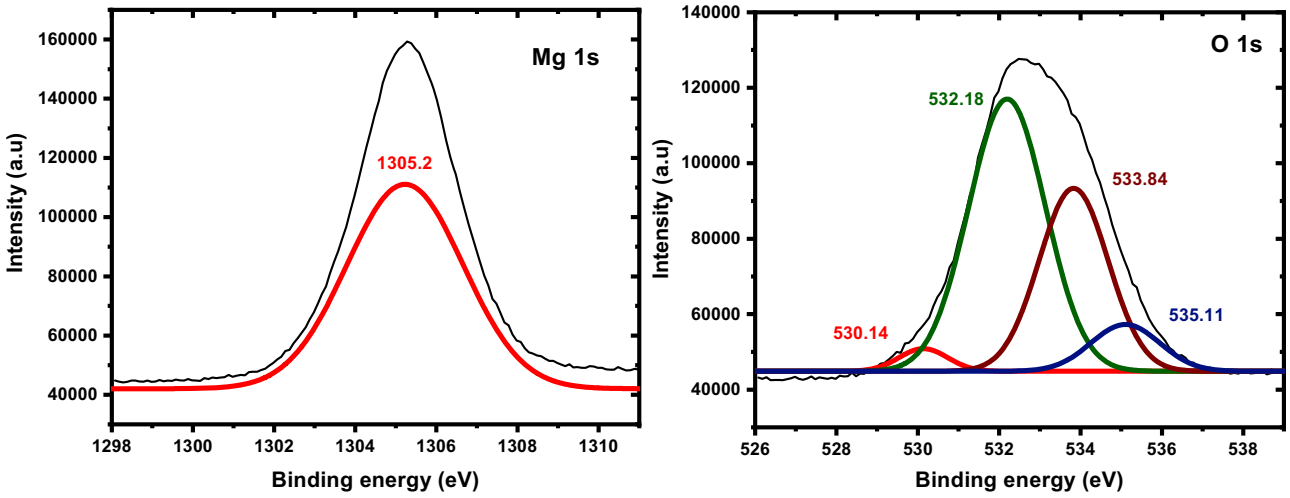

Figure 4: XPS spectra of MO1 and MO2 samples and peaks of Mg and O.

surfaces of the MgO. The observed peak corresponding to the Mg–O bond in the O 1s spectra exhibits a prominent intensity at 532.18 eV, indicating the presence of the O^{2-} ion. Furthermore, two additional peaks observed at 533.84 and 535.11 eV provide evidence of graphitic carbon within the MO2 sample. These peaks can be attributed to the graphitic C–O–C and –COOH functional groups, further supporting the presence of graphitic carbon.

3.2 Morphology

3.2.1 Field emission scanning electron microscopic analysis

The textural characteristics of the synthesised MgO nanopowder were analysed using field emission scanning electron microscopy to examine the textural characteristics. The morphological structure of MgO particles is depicted in Figure 5, illustrating the obtained result. The observed data indicate the presence of MgO particles in both samples, exhibiting a spherical morphology. Notably, the samples exhibit varying extract concentrations. The absence of alterations in the morphological composition of MgO is evident across the diverse extract concentrations employed. The particles display a uniform distribution and demonstrate specific porous attributes. The observed surface characteristics of the particles exhibit a higher probability of being smooth. Furthermore, it has been observed that MO2 particles exhibit a reduced particle size in comparison to MO1 particles. Ultimately, the interconnectivity of the particles has been achieved, effectively inhibiting the formation of particle accumulations. This desirable outcome is attributed to the interaction between bio-molecules and MgO nanoparticles, which regulate nucleation growth.

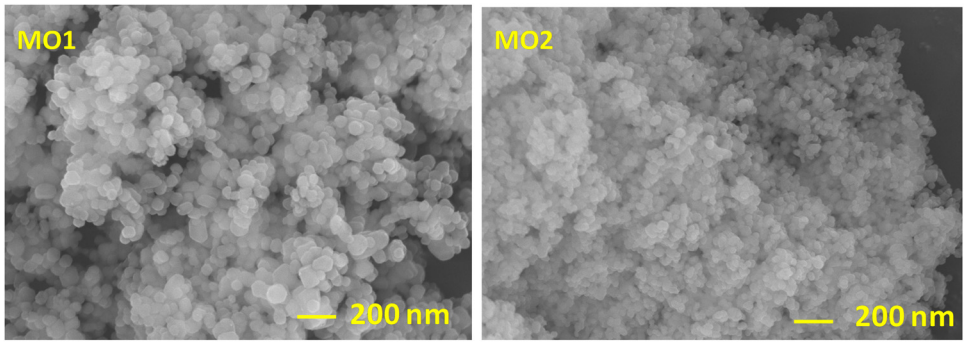

Figure 5: Surface image of MO1 and MO2 nanomaterial samples obtained from SEM analysis.

3.2.2 Energy dispersive X-ray analysis (EDAX) study

To acquire an additional understanding regarding the elemental composition and presence of carbon-based materials in MO1 and MO2 samples, EDAX spectroscopy was conducted. The results derived from the examination are visually represented in Figure 6. The presence of Mg and O in the samples is evident, and the EDAX spectra exhibit a pronounced intensity of the Mg element, indicating the formation of nanoparticles composed of MgO. Furthermore, the detected carbon traces were observed at an energy level of approximately 0.3 keV, suggesting a significantly minimal carbon content within the examined samples. Henceforth, to advance biological endeavours and facilitate subsequent investigations, we exclusively employ MO2 samples.

3.2.3 High-resolution transmission electron microscopy (HR-TEM) analysis

The utilisation of the HR-TEM technique is of utmost significance in determining nanomaterial morphology and particle size. The assessment of biological activators necessitates careful consideration of particle size and morphology, as these properties exhibit variations contingent upon the characteristics of nanomaterials. HR-TEM microscopic analysis was conducted on the MO2 sample to obtain evidence regarding particle size and morphology. Figure 7 displays the HR-TEM images of the MO2 sample, revealing the presence of MgO particles that exhibit a spherical morphology and are uniformly dispersed. The particles exhibit a high degree of interconnectivity, forming a porous structure characterised by a networked arrangement. No significant instances of agglomerated particles were observed on the surfaces under investigation. The particles exhibit a regular distribution pattern. According to the acquired data, the dimensions of the MgO nanoparticles were determined to be in the range of 50–200 nm. Moreover, the SAED pattern obtained for the MO2 sample agrees with the PXRD pattern. The samples also display well-defined and intense patterns, indicating a significant level of crystallinity. The *d* space value for the obtained particle was calculated from the TEM-SAED results and found to be 2.58 nm. It is also consistent with the PXRD results. The particle size histography exhibited the particles with an average size of 167 nm, and a spherical morphology exhibiting porous characteristics holds promise for demonstrating favourable efficacy in various biological applications.

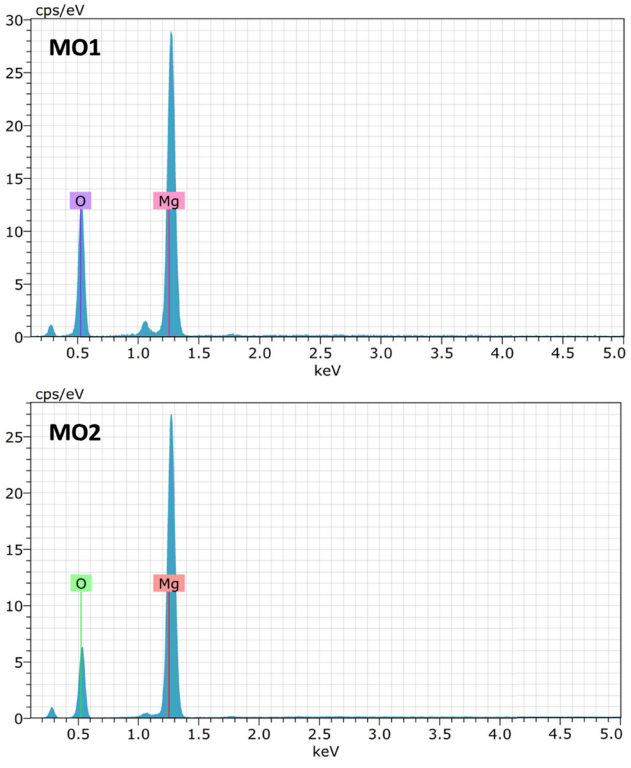

Figure 6: Chemical composition of MO1 and MO2 nanomaterials by EDAX analysis (for Mg and O elements).

3.3 Textural study

3.3.1 Brunauer-Emmett-Teller (BET) analysis

Understanding the impact of material surface area on biological activities is crucial, as it determines how they interact with various biological entities, including cells, tissues, proteins, and enzymes. Studying substances like MgO holds significant value in biological research. Enhancing the surface area significantly impacts various cellular processes, such as cell adhesion, migration, signalling, tissue regeneration, wound healing, immune responses, drug delivery, catalysis, adsorption, binding, bioavailability, and biocompatibility. This increase in available sites for interactions with neighbouring molecules or biological entities plays a crucial role in these processes. Drug delivery systems utilise materials that have enhanced surface areas, such as nanoparticles, to improve their ability to control the release of drugs and deliver them accurately to specific targets. Henceforth, it is imperative to assess the active surface area of the material before engaging in biological inquiries. The surface area of MO2 was determined using the BET nitrogen adsorption-desorption isotherms technique, with the corresponding

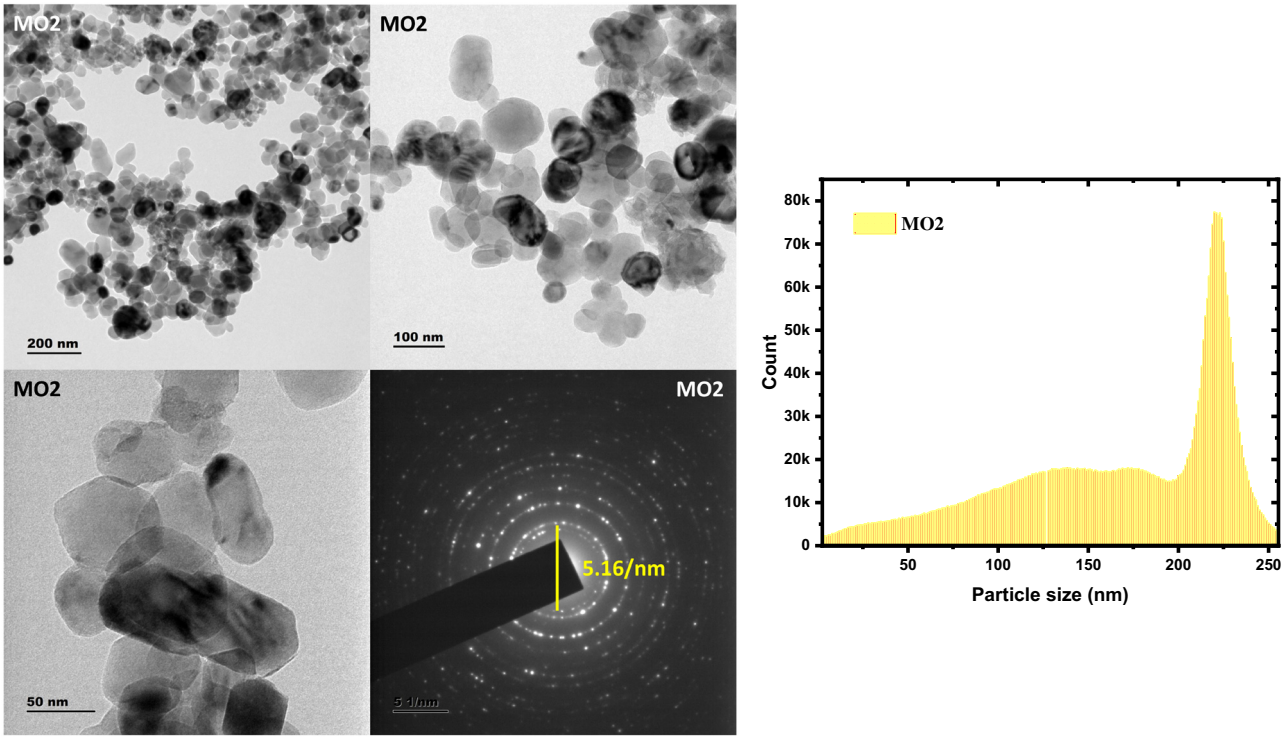

Figure 7: TEM images, SAED pattern, and particle size histogram of the MO2 nanomaterial.

outcomes presented in Figure 8. The type II isotherm commonly observed in the BET isotherm for $c > 1$ corresponds to the microspore materials. Under conditions of significantly reduced pressure, the microporous becomes saturated with nitrogen gas. The monolayer formation is initiated at the knee joint, while the subsequent multilayer formation occurs under moderate pressure conditions. Capillary condensation is observed to occur at elevated pressures. The results are presented in Figure 6, illustrating a type II isotherm curve characteristic of microporous materials. Furthermore, the determined surface area value is 23.8742 m^2/g. As determined using the Barrett-Joyner-Halenda method, the pore size distributions demonstrate a total pore volume of 0.12528 cm^3/g, while the average pore diameter is 1.7 nm. Based on the obtained results, it can be inferred that the MgO particles contain micropores with a diameter falling within the range of 1.7 nm.

3.4 Thermal study

The thermal stability of a substance is a crucial factor that influences its biological activity and practical applications. Bio-processing, preservation, medical devices, medication administration, protein denaturation, cell culture, biochemical processes, and biochemical analysis are all highly significant in the scientific realm. The thermal stability of materials utilised in bio-processing is of utmost importance in ensuring the preservation of enzyme activity, the maintenance of biological samples, and the ability to withstand sterilisation procedures. Maintaining thermal stability is of utmost importance in guaranteeing the longevity and security of medical interventions, encompassing medical apparatus, implants, and prostheses. The preservation of

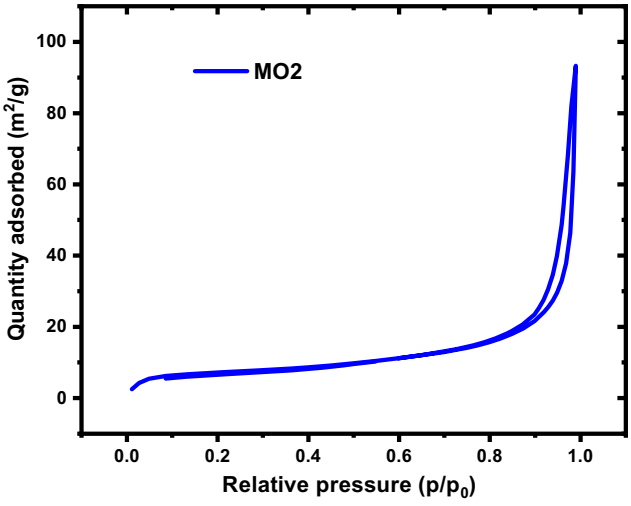

Figure 8: Results of the plot obtained from the BET analysis of MO1 and MO2 nanomaterials.

thermal stability holds significant significance within drug delivery systems, as it assumes a pivotal function in governing the kinetics and effectiveness of drug release. Therefore, the examination of the thermal properties of the synthesised materials was imperative to forecast their biological efficacy. Thermal characteristics of the synthesised MgO particles were investigated by thermogravimetric analysis (TGA), differential thermal analysis (DTA), and derivative thermogravimetry (DTG) studies, and the outcomes are presented in Figure 9. The observed phenomenon, wherein the initial decline in the degradation curve occurs at approximately 100°C, can be attributed to the process of water molecule elimination from the surface of MO2. Subsequently, the observed curve depicting the gradual deterioration occurring within the temperature range of 200–380°C, as supported by existing literature, was attributed to the transformation of magnesium hydroxide into MgO. The findings of the DTA study (Figure 9, blue line) further corroborate these assertions, as evidenced by the presence of a distinct DT curve spanning the temperature range of 200–380°C, which elucidates the phase transition occurring between $Mg(OH)_2$ and MgO. The present perspective entails thoroughly examining the $Mg(OH)_2$ composition within the MO2 sample, employing the TGA curve as a tool for analysis. The TGA curve, depicted in Figure S1, illustrates the relationship between temperature and the weight percentage of degradation. The observed phenomenon, occurring within the temperature range of 200–400°C, exhibits a distinctive curvature indicative of the transformation of $Mg(OH)_2$ into MgO. This transformation is accompanied by a concomitant reduction in weight, quantified as an 11% decrease. This observation suggests that the synthesis process did not fully convert the precursor materials into MgO. Additionally, these unconverted materials are present on the surface of MO2. Moreover, carbon traces were not detected in the TGA and DTA curves, likely due to their minimal abundance. However, the observed peak in the DTG curve, which reached a maximum temperature of 480°C, signifies the occurrence of a weight gain phenomenon attributed to the formation of carbon resulting from the reaction with carbon dioxide (CO2) [55].

3.5 Optical properties

The optical properties of materials play a crucial role in various biological processes, such as bio-sensing, imaging, phototherapy, optogenetics, bio-safety assessment, protein structure and function analysis, cellular response monitoring, and drug screening. These optical characteristics are essential in imaging techniques like fluorescence, confocal, and optical coherence tomography, which provide high-resolution observations of cells, tissues, and sub-cellular structures. By leveraging these optical properties, researchers can also manipulate neuronal activity, gene expression, and signalling pathways in specific cells, leading to significant advancements in neuroscience and studying complex biological systems. Hence, it is imperative to investigate the absorption characteristics of the nanomaterials before their application in biological processes. UV-visible absorption spectroscopy was employed to evaluate the absorption characteristics of the MO1 and MO2 samples within the wavelength range of 200–400 nm. In general, white powders composed of metal oxides demonstrate the presence of an absorption

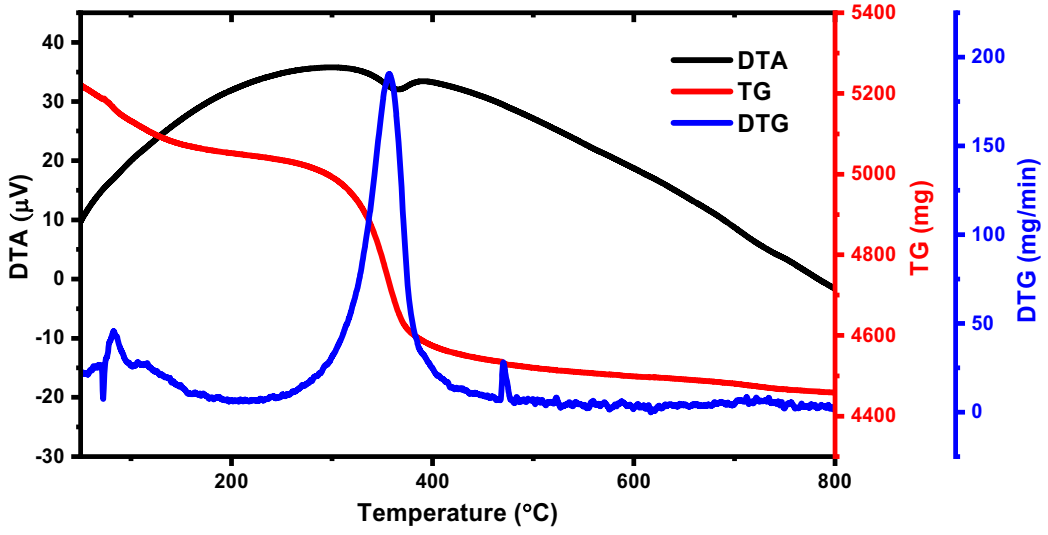

Figure 9: TG–DTA curves for MO1 and MO2 nanomaterials (black and red line). Blue line represents the DTG curve.

band within the wavelength range of 200–400 nm. These materials can be classified as semiconductors, as their energy level gap aligns with the characteristics of such materials [56–59]. Similarly, the synthesized MgO samples demonstrate a pronounced absorption peak at approximately 120 nm (Figure 10). Furthermore, the absorption edges of the MO2 samples extend around 265 nm. In contrast, the absorption edges of the MO1 samples are found at approximately 245 nm. The observed characteristics of the material suggest that its semiconductor properties exhibit a high degree of compatibility with various biological applications.

3.6 Antibacterial study

Scientists are presently investigating the effectiveness of antibacterial materials as potential agents in combating antibiotic-resistant bacteria, with the ultimate objective of improving public health. The materials above, comprised of filter paper discs containing MgO nanoparticles, were engineered to impede bacterial proliferation and establish novel colonies. The observed occurrence in which MgO particles disperse from the disc and permeate the agar medium can be accurately described as the scientific phenomenon known as "diffusion." The diffusion process leads to the emergence of a clearly defined area where microbial growth is absent, often referred to as the ZOI. The antibacterial efficacy of MO2 was assessed against Gram-negative *Klebsiella* and *Pseudomonas aeruginosa*, as well as Gram-positive *Bacillus subtilis* and *Staphylococcus albus*, utilising the disc diffusion technique. The resulting data, illustrated in Figure 11, allowed for measuring the inhibition zones (ZOI) surrounding the discs, where no observable bacterial growth was present. The observed zones in this study indicate the antibacterial activity exhibited by MO2 nanoparticles. The standard antibacterial agent, Amikacin, was employed as a control to establish a baseline comparison. The antimicrobial efficacy of MgO nanoparticles is documented in Table 1. At the same time, the accompanying visual representations of the inhibition zones resulting from the disc diffusion technique are shown in Figure 11. The bacterial structure comprises a cytoplasm, a cell wall, and a cell membrane. Gram-positive bacteria are characterised by a cell wall that is approximately 20–80 nm thick and a multilayer peptidoglycan membrane. Accordingly, the lower efficacy of MgO particles in inducing bacterial mortality can be attributed to the relatively challenging process of cell wall penetration. Similarly, the experimental findings demonstrated significantly diminished inhibition zones when tested against Gram-positive *B. subtilis* and *Staphylococcus albus* bacterial strains. The observed range of inhibition zones for Gram-positive bacteria falls within 18 to 22 mm. The results indicate that MO2 nanoparticles inhibit Gram-negative bacteria such as *Klebsiella* and *P. aeruginosa*. Notably, the observed inhibitory activity ranges from 21 to 23 mm. The Gram-negative bacteria consist of two distinct cell membranes, an outer membrane and a plasma membrane, measuring 7–8 nm in thickness. The potential ability of MgO nanoparticles to traverse the cellular membrane of the peptidoglycan polymer and subsequently exhibit antibacterial effects is high [60]. Finally, the MO2 samples exhibit a notable capacity for inhibiting the growth of Gram-negative and Gram-positive bacteria, surpassing the control group treated with Amikacin. Also, there appeared to be a marginal reduction in the ZOI when the concentration of MO2 gradually increased.

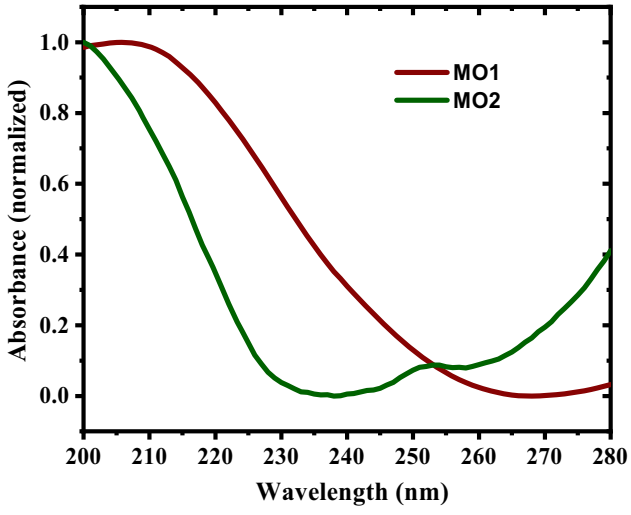

Figure 10: Absorption spectra of MO1 and MO2 nanomaterials.

3.7 Antifungal studies

Fungal diseases present substantial risks to the overall health of humans and various sectors of industry. The progression of antifungal materials, achieved through interdisciplinary collaboration, demonstrates significant potential for revolutionising the approach utilised in addressing fungal proliferation and colonisation. The materials above exhibit various applications derived from the multidisciplinary domains of materials science, biology, and medicine. The previously mentioned applications involve the utilisation of specialised coatings that have been formulated to inhibit fungal adhesion. Additionally, nanoparticles have been intricately designed to enable the controlled release of highly potent antifungal medications. By comprehensively understanding these intricate interconnections, scientists can develop novel

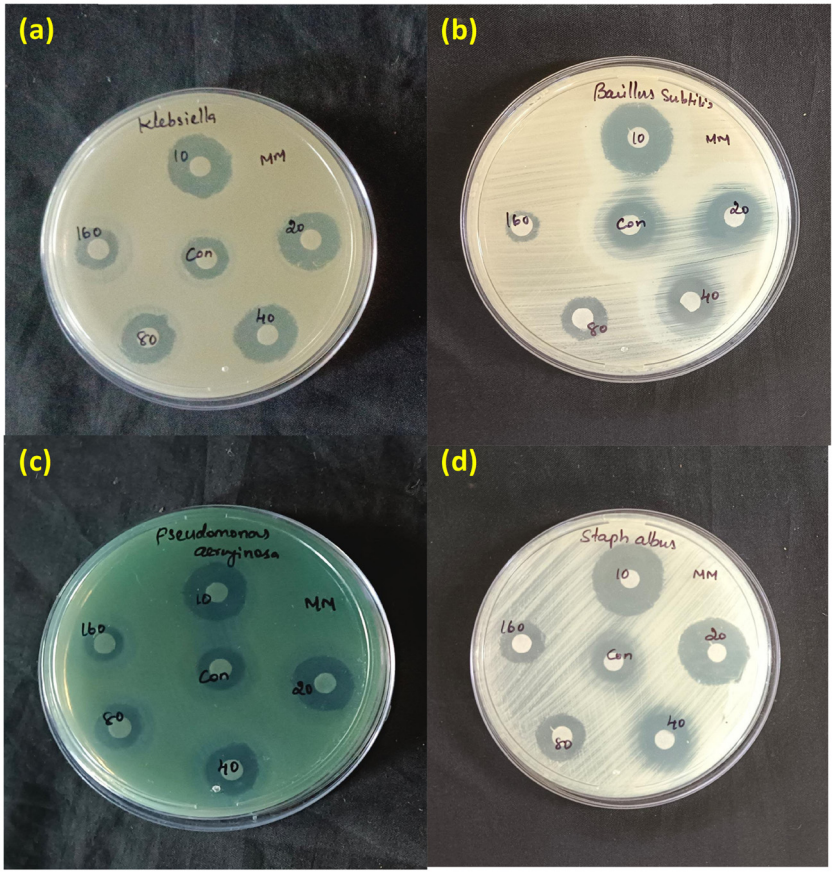

Figure 11: (a–d) shows the antibacterial activity of MO1 and MO2 nanomaterials by the disc diffusion method.

interventions to foster more robust and healthier societies. The MgO nanoparticles (MO2) were synthesised in this study using an environmentally friendly method. Their antifungal efficacy was assessed against *Candida tropicalis* and *Aspergillus niger* fungal strains. The results acquired are presented in Figure 12. In the context of performance analysis, the results are compared with *Nystatin*, a substance employed as a control. Based on the study in Table 2, the antifungal efficacy of MO2 exhibits a notably elevated level compared to the control *Nystatin* standard, specifically in its impact on *Candida tropicalis*. The disparity between the two agents amounts to approximately 6 mm. In the context of *Aspergillus niger*, the observed activity exhibited a marginal decrease in comparison to the control. The observed discrepancies in fungal performances can be attributed to the extent of cell wall penetration, which is contingent upon variations in cell thickness. A prototypical fungal organism comprises a conglomeration of tubular and ramified filaments enveloped by a sturdy cellular barrier. The elongated structures, called hyphae (individually known as hypha), exhibit repetitive

Table 1: Antibacterial performance of MO1 and MO2

Bacteria	ZOI (mm)					Control (Amikacin)
	Concentration of MO2 (µg/mL)					
	10	20	40	80	160	
Klebsiella	20	18	16	15	13	13
Pseudomonas aeruginosa	18	16	15	13	11	13
Bacillus subtilis	21	19	15	13	09	16
Staphylococcus albus	23	21	19	15	13	15

branching patterns, forming an intricate, radially expanding interconnected system known as mycelium. This mycelium constitutes the thallus, an undifferentiated organism body characteristic of a prototypical fungus. The inability of MgO nanoparticles to traverse the inflexible cellular membrane potentially accounts for their lack of efficacy against fungal organisms [8]. From this perspective, the observed limited efficacy of MO2 against *A. niger* can be attributed to the presence of a robust cell wall in the fungal strain, which restricts the penetration of MgO particles. However, it is observed that *C. tropicalis* exhibits a comparatively augmented cell wall structure, which can be attributed to the fact that the process of cell wall penetration requires a reduced amount of force.

Table 2: Fungal performance of MO1 and MO2

Fungus	ZOI (mm)				Control (Nystatin)
	Concentration of MO2 (µg/mL)				
	10	20	40	80	
Candida tropicalis	16	13	12	08	10
Aspergillus niger	15	17	11	10	17

3.8 Anti-inflammation study

The amalgamation of materials science, immunology, and medicine has resulted in the emergence of anti-inflammatory materials, exhibiting substantial potential in revolutionising the management of inflammation-associated ailments. A diverse array of materials, encompassing a variety of surfaces and nanoparticles, show the capacity to mitigate inflammatory responses and efficiently administer potent pharmaceutical agents. Researchers are presently engaged in examining the mechanisms by which they engage with the immune system of the human organism. This endeavour has given rise to innovative medical implants and wearable device advancements. The anti-inflammatory properties of the synthesised MgO nanoparticles were assessed to determine their efficacy in mitigating inflammation. The obtained results were subsequently subjected to a comparative analysis with those of a widely used anti-inflammatory pharmaceutical agent, namely the diclofenac standard (Figure 13). The tables provided display the percentage inhibition observed for both the standard drug and MgO nanoparticles. The experimental findings indicate that MgO nanoparticles, synthesised using a green method, exhibit a more significant percentage of inhibition than the standard diclofenac. Diclofenac-derived pharmaceuticals exhibited a notable decrease in protein denaturation, with reductions of approximately 7.8% observed at a concentration of 6.2 µg/mL and a more substantial decrease of up to 78% observed at 100 µg/mL. The IC_{50} of diclofenac control ranges from 6.2 mg/mL to 100 µg/mL, with a specific value of 49.68 µg/mL. The observed effects of MgO nanoparticles on protein denaturation were quantified, revealing a reduction of up to 9% at a concentration of 6.2 µg/mL and a more substantial decrease of up to 55.45% at 200 µg/mL. The IC_{50} values of MgO nanoparticles were determined to be 164.15 at 200 and 6.2 µg/mL at a 9.98 µg/mL concentration. Figure 13 presents the IC_{50} values of the standard compound diclofenac and the sample nanoparticles denoted as MO2. The mean inhibition of protein denaturation for diclofenac is observed to be 49.68, while for the MO2 sample, it is found to be 164.15.

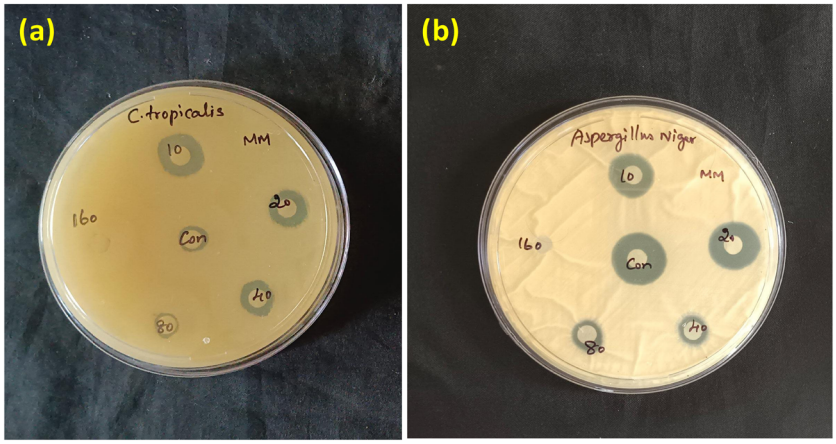

Figure 12: (a, b) shows the antifungal activity of MO1 and MO2 nanomaterials by the disc diffusion method.

The extensive diversity observed in this study elucidates the inherent capacity of MO2 nanoparticles to exhibit antifungal properties.

3.9 Anti-diabetic activity of α-glucosidase inhibition assay

The development of multidisciplinary anti-diabetic materials presents a promising opportunity for revolutionary advancements in the management and treatment of diabetes. Numerous materials are being examined for their prospective utilisation in implantable devices and wearable technologies. The materials above exhibit a broad spectrum of properties, encompassing various biomaterials specifically engineered for controlled drug release and exact glucose monitoring systems. Scientists aim to optimise glucose regulation and treatment regimens and enhance the well-being of individuals with diabetes by comprehensively understanding these interconnections. In the current study, the MO2 nanoparticles that were synthesised are subjected to an assay for α-glucosidase inhibition and an assay for -amylase to assess their potential diabetic properties. The data presented in Figure 14 originate from an assay measuring the inhibition of α-glucosidase, an enzyme commonly targeted to evaluate compound inhibitory potential. The enzyme mentioned above serves a pivotal function in carbohydrate digestion and has been identified as a prime target for pharmaceutical interventions aimed at diabetes management. These assays aim to identify compounds that can efficiently impede glucosidase activity, as this has the potential to modulate glycaemic control. The compound under investigation, acarbose, exhibits noteworthy inhibitory activity against α-glucosidase. At the maximum concentration examined (100 µg/mL), it effectively suppresses approximately 94% of the enzyme's catalytic function. Figure 14 illustrates a dose-dependent relationship wherein the observed response is contingent upon the concentration of acarbose. Specifically, as the concentration of acarbose increases, the inhibitory impact on α-glucosidase activity becomes increasingly conspicuous. Based on the measured IC_{50} value of 16.58 g/mL, it can be concluded that acarbose exhibits significant potency as an α-glucosidase inhibitor. The data for MO2 have been derived from the α-glucosidase inhibition assay, encompassing details such as the concentrations of the samples, optical density (OD)

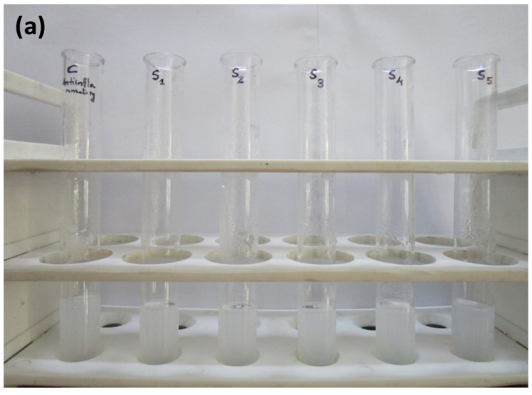

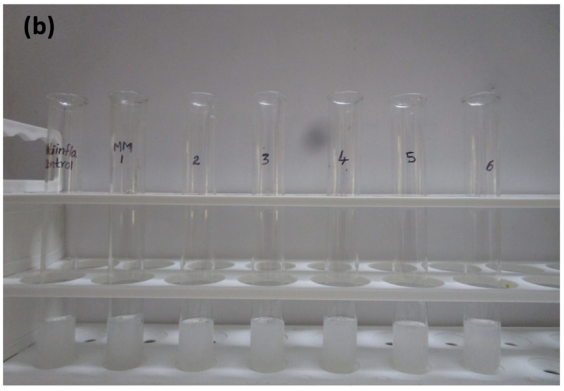

(c)

Standard	Concentration (µg/ml)	OD at 660 nm	% of Inhibition
Control	-	0.787	
Diclofenac	6.25	0.725	7.88
	12.5	0.661	16.01
	25	0.545	30.75
	50	0.368	53.24
	100	0.125	84.12
IC50	49.68		

(d)

Sl. No.	Sample code	Concentration (µg/ml)	OD at 660 nm	% of Inhibition
1	Control	-	0.862	
	MM	6.25	0.776	9.98
		12.5	0.728	15.55
		25	0.654	24.13
		50	0.585	32.13
		100	0.514	40.37
		200	0.384	55.45
	IC 50	164.15		

Figure 13: The anti-inflammatory activity of MO1 (a) and MO2 (b) nanomaterials (performance compared with diclofenac standard). (c) and (d) activity data of the inflammation studies.

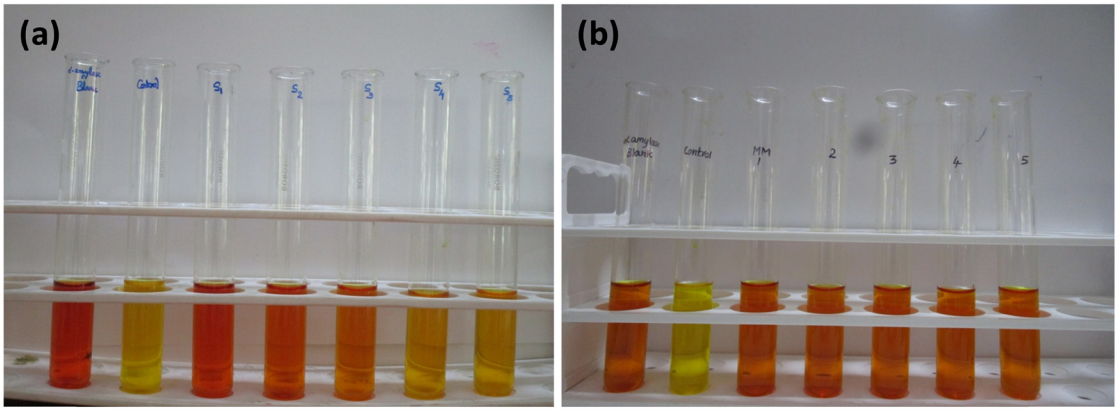

(c)

Sample code	Concentration (µg/ml)	OD at 400nm	% of Inhibition
Blank	-	0.724	-
Control	-	0.032	-
Acarbose (standard)	6.25	0.584	20.23
	12.5	0.451	39.45
	25	0.216	73.41
	50	0.138	84.68
	100	0.074	93.93
IC 50	16.58		

(d)

Sl. No.	Sample code	Concentration (µg/ml)	OD at 400nm	% of Inhibition
1	Blank	-	1.445	
	Control	-	0.012	
	MM	1.5	1.429	1.12
		3.125	1.374	4.95
		6.25	1.316	9.00
		12.5	1.296	10.40
		25	1.083	25.26
		50	0.975	32.80
		100	0.876	39.71
Expected IC 50		152.55		

Figure 14: The anti-diabetic activity of MO1 (a) and MO2 (b) nanomaterials (performance compared with the acarbose standard). (c) and (d) Activity data of the diabetic studies.

measurements at a wavelength of 400 nm, and the corresponding percentage of inhibition. The term "blank" denotes a control devoid of any compound, exhibiting an OD reading of 1.445. "Control" denotes a negative control or baseline exhibiting an OD measurement of 0.012. This value is notably lower than that of the blank. The compound under investigation is MO2. As the concentration of MO2 is augmented, there is a corresponding decrease in the OD readings. This decrease is indicative of the inhibition of beta-glucosidase activity. The observed phenomenon aligns with the anticipated behaviour of an α-glucosidase inhibitor. The observed inhibition phenomenon positively correlates with the concentration of MO2, suggesting a response dependent on the dosage administered. It can be inferred that elevated levels of MO2 exhibit enhanced efficacy in inhibiting beta-glucosidase. The calculated IC_{50} value is anticipated to be 152.55 g/mL. The concentration at which it is estimated that MO2 would exert a 50% inhibitory effect on beta-glucosidase activity is presented now. The data analysis indicates that the MO2 compound exhibits noteworthy inhibitory activity against glucosidase. The observed phenomenon exhibits a dose-dependent response, wherein higher concentrations elicit a more pronounced inhibitory effect. Based on the anticipated IC_{50} value of 152.55 g/mL, it can be inferred that this compound exhibits a more significant potential as an α-glucosidase inhibitor than acarbose. Consequently, further investigation is warranted into its potential as an agent for managing diabetes. This observation implies that MO2 exhibits promising prospects as an anti-diabetic agent due to its capacity to efficiently decelerate the process of carbohydrate digestion and absorption, thereby resulting in enhanced regulation of blood glucose levels.

4 Conclusions

We have successfully utilised the *Vitis vinifera* plant to produce MgO nanoparticles, a unique bio-reducing agent. Using PXRD and FT-IR analysis techniques, the nanoparticles were characterised to determine their crystal structure, which was found to be FCC. C–N/C–O and N–H functional groups derived from carbon molecules were also observed. The purity of the MgO sample was confirmed through Raman spectroscopy analysis. Thermal stability was evaluated using thermogravimetric and differential thermal analyses, which revealed the presence of carbon. Upon

analysing the surface morphology, it was found that there were tiny spherical particles uniformly distributed throughout, each measuring less than 50 nm in size. These particles also exhibited a porous structure. Jana and her colleagues have discovered that an ethanolic extract from *Vitis vinifera* canes can assist in the production of silver nanoparticles. The synthesis process required 10% of the extract and 1 mM of silver nitrate. The *Z*-average of the silver nanoparticles was determined to be 68.2 nm, while their zeta potential was observed to be −30.4 mV. These silver nanoparticles effectively suppressed the growth of planktonic cells in all strains of *P. aeruginosa* at doses below 5% v/v. In addition, they effectively inhibited the growth of biofilms at concentrations below 6% v/v. In addition, the minimum bactericidal concentration was found to range from 10 to 16% v/v. Utilising wine farm waste in this study has proven to be a sustainable and cost-effective method for producing silver nanoparticles with remarkable antibacterial properties. Researchers found that MgO nanoparticles have a strong toxic effect on *Aspergillus niger*. The experiment showed a gradual inhibitory impact when using 0.5 and 1.25% concentrations. The inhibitory efficacy of the poisoned food technique reached 66.6 and 100%, respectively. Experiments were conducted to evaluate the antibacterial and antifungal properties of the MgO nanomaterials. Like a materials scientist, the amikacin control displayed a significant inhibition zone of around 15 mm against the bacteria. However, the activity was greatly enhanced by the presence of MgO nanoparticles. Researchers examined the anti-inflammatory properties of MgO (MO2) nanoparticles by comparing them with diclofenac, a commonly used anti-inflammatory drug. The study found that the presence of MgO (MM or MO2) nanoparticles led to a notable increase in protein denaturation, indicating a potential for anti-inflammatory activity. The anti-diabetic activity was also evaluated, and the IC_{50} value of 152 was compared to the standard acarbose. This comparison highlights the potential of MgO nanoparticles in effectively regulating diabetes and inflammation progression.

Acknowledgments: The authors thank the National Engineering College and St. Jude's College for providing lab facilities.

Funding information: This project was supported by Researchers Supporting Project Number (RSP-2025R7) at King Saud University, Riyadh, Saudi Arabia.

Author contributions: All authors have accepted responsibility for the entire content of this manuscript and approved its submission.

Conflict of interest: The authors state no conflict of interest.

Data availability statement: The datasets generated and/or analysed during the current study are available from the corresponding author on reasonable request.

References

[1] Roduner E. Size matters: why nanomaterials differ. Chem Soc Rev. 2006;35:583–92.
[2] Gogotsi Y. Nanomaterials handbook. Boca Raton: CRC Press; 2006.
[3] Khot LR, Sankaran S, Maja JM, Ehsani R, Schuster EW. Applications of nanomaterials in agricultural production and crop protection: a review. Crop Prot. 2012;35:64–70.
[4] Mazari SA, Ali E, Abro R, Khan FSA, Ahmed I, Ahmed M, et al. Nanomaterials: Applications, waste-handling, environmental toxicities, and future challenges–A review. J Environ Chem Eng. 2021;9:105028.
[5] Gajanan K, Tijare SN. Applications of nanomaterials. Mater Today: Proc. 2018;5:1093–6.
[6] Barreto JA, O'malley W, Kubeil M, Graham B, Stephan H, Spiccia L. Nanomaterials: applications in cancer imaging and therapy. Adv Mater. 2011;23:H18–40.
[7] Vinayagam R, Pai S, Varadavenkatesan T, Pugazhendhi A, Selvaraj R. Characterization and photocatalytic activity of ZnO nanoflowers synthesized using Bridelia retusa leaf extract. Appl Nanosci. 2023;13:493–502. doi: 10.1007/s13204-021-01816-5.
[8] Emima Jeronsia J, Ragu R, Sowmya R, Mary AJ, Jerome Das S. Comparative investigation on Camellia Sinensis mediated green synthesis of Ag and Ag/GO nanocomposites for its anticancer and antibacterial efficacy. Surf Interfaces. 2020;21:100787.
[9] Vinayagam R, Nagendran V, Goveas LC, Narasimhan MK, Varadavenkatesan T, Chandrasekar N, et al. Structural characterization of marine macroalgae derived silver nanoparticles and their colorimetric sensing of hydrogen peroxide. Mater Chem Phys. 2024;313:128787.
[10] Baig N, Kammakakam I, Falath W. Nanomaterials: A review of synthesis methods, properties, recent progress, and challenges. Mater Adv. 2021;2:1821–71.
[11] Kolahalam LA, Viswanath IK, Diwakar BS, Govindh B, Reddy V, Murthy YL. Review on nanomaterials: Synthesis and applications. Mater Today: Proc. 2019;18:2182–90.
[12] Vinayagam R, Pai S, Murugesan G, Varadavenkatesan T, Selvaraj R. Synthesis of photocatalytic zinc oxide nanoflowers using Peltophorum pterocarpum pod extract and their characterization. Appl Nanosci. 2023;13:847–57. doi: 10.1007/s13204-021-01919-z.
[13] Venkatesham M, Ayodhya D, Madhusudhan A, Veera Babu N, Veerabhadram G. A novel green one-step synthesis of silver nanoparticles using chitosan: catalytic activity and antimicrobial studies. Appl Nanosci. 2014;4:113–9.
[14] Shaikh WA, Chakraborty S, Owens G, Islam RU. A review of the phytochemical mediated synthesis of AgNP (silver nanoparticle): The wonder particle of the past decade. Appl Nanosci. 2021;11:2625–60.
[15] Chowdhury R, Saini SK, Roy J. Bio-fabrication of TiO2 nanomaterials and their applications in electronics devices. J Electron Mater. 2021;50:6087–101.

[16] Thunugunta T, Reddy AC, Reddy DCL. Green synthesis of nanoparticles: current prospectus. Nanotechnol Rev. 2015;4:303–23.
[17] Aravind M, Amalanathan M, Mary MSM. Synthesis of TiO_2 nanoparticles by chemical and green synthesis methods and their multifaceted properties. SN Appl Sci. 2021;3:1–10.
[18] Basnet P, Chanu TI, Samanta D, Chatterjee S. A review on biosynthesized zinc oxide nanoparticles using plant extracts as reductants and stabilizing agents. J Photochem Photobiol B: Biol. 2018;183:201–21.
[19] Chaudhary RG, Bhusari GS, Tiple AD, Rai AR, Somkuvar SR, Potbhare AK, et al. Metal/metal oxide nanoparticles: toxicity, applications, and future prospects. Curr Pharm Des. 2019;25:4013–29.
[20] Augustine R, Hasan A. Emerging applications of biocompatible phytosynthesized metal/metal oxide nanoparticles in healthcare. J Drug Delivery Sci Technol. 2020;56:101516.
[21] Tao F. Excavation of precious-metal-based alloy nanoparticles for efficient catalysis. Angew Chem Int Ed. 2016;55:15212–4.
[22] Desoize B. Metals and metal compounds in cancer treatment. Anticancer Res. 2004;24:1529–44.
[23] Albarede F, Telouk P, Balter V. Medical applications of isotope metallomics. Rev Mineral Geochem. 2017;82:851–85.
[24] Chong Y, Huang J, Xu X, Yu C, Ning X, Fan S, et al. Hyaluronic acid-modified Au–Ag alloy nanoparticles for radiation/nanozyme/Ag^+ multimodal synergistically enhanced cancer therapy. Bioconjugate Chem. 2020;31:1756–65.
[25] Song Y, Qu Z, Li J, Shi L, Zhao W, Wang H, et al. Fabrication of the biomimetic DOX/Au@ Pt nanoparticles hybrid nanostructures for the combinational chemo/photothermal cancer therapy. J Alloy Compd. 2021;881:160592.
[26] Chavali MS, Nikolova MP. Metal oxide nanoparticles and their applications in nanotechnology. SN Appl Sci. 2019;1:607.
[27] Akilan M, Ragu R, Angelena JP, Das SJ. Enhancement in mechanical, optical, SHG, photoacoustic and Z-scan studies on pure and crystal violet dye doped L-proline cadmium chloride single crystal for nonlinear optical applications. J Mater Sci: Mater Electron. 2019;30:3655–62. doi: 10.1007/s10854-018-00645-7.
[28] Ragu R, Mageshwari PSL, Akilan M, Angelena JP, Das SJ. Enrich mechanical, photo-acoustic, SHG and Z-scan studies on pure and crystal violet dye (CV) incorporated sodium acid phthalate crystal for optical applications. J Mater Sci: Mater Electron. 2019;30:1670–6. doi: 10.1007/s10854-018-0438-6.
[29] Kim I-S, Baek M, Choi S-J. Comparative cytotoxicity of Al2O3, CeO2, TiO2 and ZnO nanoparticles to human lung cells. J Nanosci Nanotechnol. 2010;10:3453–8.
[30] Aravind M, Amalanathan M, Mary MSM, Parvathiraja C, Alothman AA, Wabaidur SM, et al. Enhanced photocatalytic and biological observations of green synthesized activated carbon, activated carbon doped silver and activated carbon/silver/titanium dioxide nanocomposites. J Inorg Organomet Polym Mater. 2022;32(1):267–79.
[31] Chinthala M, Balakrishnan A, Venkataraman P, Manaswini Gowtham V, Polagani RK. Synthesis and applications of nano-MgO and composites for medicine, energy, and environmental remediation: a review. Environ Chem Lett. 2021;19:4415–54.
[32] Seitz J-M, Eifler R, Bach F-W, Maier HJ. Magnesium degradation products: effects on tissue and human metabolism. J Biomed Mater Res Part A. 2014;102:3744–53.
[33] Yi Y, Liska M, Al-Tabbaa A. Properties of two model soils stabilized with different blends and contents of GGBS, MgO, lime, and PC. J Mater Civ Eng. 2014;26:267–74.
[34] Abdallah Y, Ogunyemi SO, Abdelazez A, Zhang M, Hong X, Ibrahim E, et al. The green synthesis of MgO nano-flowers using Rosmarinus officinalis L.(Rosemary) and the antibacterial activities against Xanthomonas oryzae pv. oryzae. BioMed Res Int. 2019;2019:1–8.
[35] Stankic S, Bernardi J, Diwald O, Knözinger E. Optical surface properties and morphology of MgO and CaO nanocrystals. J Phys Chem B. 2006;110:13866–71.
[36] Wahid F, Zhao X-J, Jia S-R, Bai H, Zhong C. Nanocomposite hydrogels as multifunctional systems for biomedical applications: Current state and perspectives. Compos Part B: Eng. 2020;200:108208.
[37] Khalid A, Norello R, Abraham AN, Tetienne JP, Karle TJ, Liu EWC, et al. Biocompatible and biodegradable magnesium oxide nanoparticles with in vitro photostable near-infrared emission: Short-term fluorescent markers. Nanomaterials. 2019;9:1360.
[38] Waghchaure RH, Adole VA. Biosynthesis of metal and metal oxide nanoparticles using various parts of plants for antibacterial, antifungal and anticancer activity: A review. J Indian Chem Soc. 2023;100:100987.
[39] Algethami FK, Katouah HA, Al-Omar MA, Almehizia AA, Amr AEGE, Naglah AM, et al. Facile synthesis of magnesium oxide nanoparticles for studying their photocatalytic activities against orange G Dye and biological activities against some bacterial and fungal strains. J Inorg Organomet Polym Mater. 2021;31:2150–60.
[40] Sharma BK, Mehta BR, Chaudhari VP, Shah EV, Mondal Roy S, Roy DR. Green synthesis of dense rock MgO nanoparticles using carica papaya leaf extract and its shape dependent antimicrobial activity: Joint experimental and DFT investigation. J Clust Sci. 2022;33:1667–75.
[41] Fatiqin A, Amrulloh H, Simanjuntak W. Green synthesis of MgO nanoparticles using Moringa oleifera leaf aqueous extract for antibacterial activity. Bull Chem Soc Ethiopia. 2021;35:161–70.
[42] Dabhane H, Ghotekar S, Zate M, Kute S, Jadhav G, Medhane V. Green synthesis of MgO nanoparticles using aqueous leaf extract of Ajwain (Trachyspermum ammi) and evaluation of their catalytic and biological activities. Inorg Chem Commun. 2022;138:109270.
[43] Saka A, Jule LT, Gudata L, Gindaba A, Abdisa SS, Nagaprasad N, et al. Green synthesis of Datura stramonium (Asaangira) leaves infusion for antibacterial activity through magnesium oxide (MgO) nanoparticles. Adv Mater Sci Eng. 2022;2022:1–8.
[44] Ahmad A, Khan M, Khan S, Luque R, Almutairi TM, Karami AM. Bioconstruction of MgO nanoparticles using Texas sage plant extract for catalytical degradation of methylene blue via photocatalysis. Int J Environ Sci Technol. 2023;20:1451–62.
[45] Vijayakumar S, Chen J, González Sánchez ZI, Tungare K, Bhori M, Durán-Lara EF, et al. Moringa oleifera gum capped MgO nanoparticles: Synthesis, characterization, cyto-and ecotoxicity assessment. Int J Biol Macromol. 2023;233:123514.
[46] Dhage SS, Biradar DP, Aladakatti YR, Chandashekhar SS, Hosamani R. Green synthesis and characterization of magnesium oxide nanoparticles from leaf extracts of Amaranthus retroflexus and Azadirachta indica. Int J Env Clim Change. 2023;13:214–9.
[47] Jeevanandam J, Rodrigues J. Sustainable synthesis of bionanomaterials using non-native plant extracts for maintaining ecological balance: A computational bibliography analysis. J Environ Manag. 2024;358:120892.

[48] Ali S, Sudha KG, Thirumalaivasan N, Ahamed M, Pandiaraj S, Rajeswari VD, et al. Green synthesis of magnesium oxide nanoparticles by using abrus precatorius bark extract and their photocatalytic, antioxidant, antibacterial, and cytotoxicity activities. Bioengineering. 2023;10:302.
[49] Arun J, Nachiappan S, Rangarajan G, Alagappan RP, Gopinath KP, Lichtfouse E. Synthesis and application of titanium dioxide photocatalysis for energy, decontamination and viral disinfection: A review. Environ Chem Lett. 2023;21(1):339–62.
[50] Rezić I. Nanoparticles for biomedical application and their synthesis. Polymers. 2022;14:4961.
[51] Elmaidomy AH, Mohamad SA, Abdelnaser M, Yahia R, Mokhtar FA, Alsenani F, et al. Vitis vinifera leaf extract liposomal Carbopol gel preparation's potential wound healing and antibacterial benefits: in vivo, phytochemical, and computational investigation. Food Funct. 2023;14:7156–75.
[52] Pandey V, Pant KK, Upadhyayula S. Combustion induced synthesis of multicomponent Cu-based catalysts for autocatalytic CO hydrogenation to methanol in a three-phase reactor system. React Chem Eng. 2023;8:442–54.
[53] Nzekoue FK, Kouamo Nguefang ML, Alessandroni L, Mustafa AM, Vittori S, Caprioli G. Grapevine leaves (Vitis vinifera): Chemical characterization of bioactive compounds and antioxidant activity during leave development. Food Biosci. 2022;50:102120.
[54] Zahir MH, Rahman MM, Irshad K, Rahman MM. Shape-stabilized phase change materials for solar energy storage: MgO and $Mg(OH)_2$ mixed with polyethylene glycol. Nanomaterials. 2019;9:1773.
[55] Qingge F, Huidong C, Haiying L, Siying Q, Zheng L, Dachao M, et al. Synthesis and structural characteristics of high surface area TiO2 aerogels by ultrasonic-assisted sol–gel method. Nanotechnology. 2018;29(7):075702.
[56] Althomali RH, Jabbar HS, Kareem AT, Abdullaeva B, Abdullaev SS, Alsalamy A, et al. Various methods for the synthesis of $NiTiO_3$ and $ZnTiO_3$ nanomaterials and their optical, sensor and photocatalyst potentials: a review. Inorg Chem Commun. 2023;111493.
[57] Shai LJ, Masoko P, Mokgotho MP, Magano SR, Mogale AM, Boaduo N, et al. Yeast alpha glucosidase inhibitory and antioxidant activities of six medicinal plants collected in Phalaborwa, South Africa. South Afr J Botany. 2010;76(3):465–70.
[58] Bindhu MR, Umadevi M, Micheal MK, Arasu MV, Al-Dhabi NA. Structural, morphological and optical properties of MgO nanoparticles for antibacterial applications. Mater Lett. 2016;166:19–22.
[59] Bindhu MR, Umadevi M, Esmail GA, Al-Dhabi NA, Arasu, MV. Green synthesis and characterization of silver nanoparticles from Moringa oleifera flower and assessment of antimicrobial and sensing properties. J Photochem Photobiol B: Biol. 2020;205:111836.
[60] Aslinjensipriya A, Reena RS, Infantiya SG, Ragu R, Jerome Das S. Uncovering the replacement of Zn2+ ions on nano-structural, opto/magneto/electrical, antibacterial and antifungal attributes of nickel oxide nanoparticles via sol-gel strategy. J Solid State Chem. 2022;311:123146.